

Intrinsic accuracy in 3-dimensional photoemission band mapping

V. N. Strocov*

Experimentalphysik II, Universität Augsburg, D-86135 Augsburg,
Germany

(November 20, 2018)

Fundamental principles of mapping 3-dimensional quasiparticle dispersions in the valence band using angle-resolved photoemission spectroscopy are discussed. Such mapping is intrinsically limited in accuracy owing to damping of the final states, resulting in equivalent broadening in the surface-perpendicular wavevector. Mechanisms of the intrinsic accuracy are discussed in depth based on a physically transparent picture involving interplay of the final- and initial-state spectral functions, and illustrated by photoemission simulations and experimental examples. Other interesting effects of 3-dimensional dispersions include 'ghost' photoemission peaks outside the Fermi surface and finite peak width at the Fermi level. Finally, optimization of the experiment on the intrinsic accuracy is discussed.

Keywords: Bandstructure; Photoemission; 3-dimensional effects; Final states; Intrinsic effects

I. INTRODUCTION: WHY INTRINSIC ACCURACY?

The quasiparticle bandstructure $E(\mathbf{k})$, which reflects the peaks of the spectral function $A(E, \mathbf{k})$ depending on energy and wavevector \mathbf{k} , is the key property of the crystalline solids. Angle-resolved photoemission (PE) spectroscopy (for reviews see, e.g., [1,2]) is the main experimental method to map $E(\mathbf{k})$ with resolution in energy E and, in principle, in the 3-dimensional \mathbf{k} (*3D band mapping*). This is based on conservation of \mathbf{k} in the process of photoexcitation from the occupied initial state to unoccupied final state in the bulk of the crystal. However, the PE experiment is inherently performed on the crystal terminated by the surface. By virtue of the remaining surface-parallel periodicity, the surface-parallel wavevector \mathbf{k}_{\parallel} is conserved in the whole system and can be determined from the surface-parallel vacuum wavevector \mathbf{K}_{\parallel} with the accuracy limited only by instrumental resolution. As the surface-perpendicular periodicity is however broken, the surface-perpendicular wavevector k_{\perp} is not conserved in the whole system and can not be directly determined. Control over k_{\perp} is therefore a fundamental problem of 3D band mapping.

The control over k_{\perp} has two aspects. First, k_{\perp} is distorted when the photoelectrons exit from the bulk of the solid into vacuum. As k_{\perp} is conserved in the very photoexcitation process in the bulk, it can nevertheless be recovered if the k_{\perp} -dispersion of the final state $E^f(k_{\perp})$ or that of the initial state $E^i(k_{\perp})$ back in the bulk is known.

Commonly an empirical free-electron-like approximation is used here for the final states, though the accuracy of this can often be insufficient. Nevertheless, the true quasiparticle $E^f(k_{\perp})$ including the non-free-electron and self-energy effects in the final state can be determined using very-low-energy electron diffraction (VLEED) spectroscopy (see [3–5] and references therein) based on that the PE final states, as proved by the one-step theory of PE, are the time-reversed LEED states [6,7]. It is a common point of view that knowledge of the final-state $E(\mathbf{k})$ exhaust the whole problem of 3D band mapping. Indeed, variation of the final-state energy E^f in the PE experiment (commonly achieved by variation of the photon energy $h\nu$) would through known $E^f(k_{\perp})$ be translated into variations of k_{\perp} , and accurate 3D mapping of the occupied $E(\mathbf{k})$ would be performed.

There is another aspect however. Due to inelastic absorption and elastic reflection from the crystal potential the PE final state is intrinsically damped towards interior of the solid [6,7]. Such a confinement in the surface-perpendicular coordinate is equivalent, by the uncertainty principle, to certain *intrinsic broadening in k_{\perp}* . The PE signal via this final state is then formed by all initial states within the k_{\perp} -broadening interval, and the PE peak reflects an average of the quasiparticle $E^i(k_{\perp})$ in the valence band. A difference of the measured averaged k_{\perp} -dispersion from the true $E^i(k_{\perp})$ limits *intrinsic accuracy* of 3D band mapping. It is borne by fundamental physics of the PE process, and can not be improved instrumentally.

The intrinsic accuracy appears thus as an *extrinsic* factor to the excited-state self-energy effects as deviations of the quasiparticle excited-state $E(\mathbf{k})$, measured in the ideal PE experiment with undamped final states, from the ground-state bandstructure.

The intrinsic accuracy problem has in pieces been tackled in quite a few papers. Here, my aim is to delineate an entire concept, including essential physics and mechanisms of the intrinsic accuracy, and unveil its non-trivial effects encountered in the PE experiment. The concept is built upon a simple picture involving interplay of the final- and initial-state spectral functions, which gives a clearer physical insight compared to the explicit one-step PE theory with its heavy computational machinery. Finally, I discuss optimization of the PE experiment with respect to the intrinsic accuracy of 3D band mapping.

II. BASIC PHYSICS OF THE PE PROCESS

In the following analysis of the PE process it is implied that $E(\mathbf{k})$ is the quasiparticle bandstructure, already incorporating the excited-state self-energy effects. We will neglect the surface effects and concentrate on the bulk derived states with significant dispersion in k_{\perp} (so-called *3D states*). The ideal E - and \mathbf{k}_{\parallel} -resolution of the PE experiment is assumed.

A. Initial and final states of PE

First we will recall physics of the PE initial and final states based on the ideas from [1,2,8]. For simplicity we will assume that their wavefunctions have only one Bloch wave constituent.

The final-state wavefunction is the time-reversed LEED wavefunction. As sketched in Fig.1 (the upper panels represent the final state), the wavefunction is described by a Bloch wave which is damped in the surface-perpendicular direction r_{\perp} towards the crystal interior [3,5,9,10]. There are two sources of such damping: 1) inelastic absorption, expressed by absorption potential V_i connected with the electron lifetime as $2V_i = \hbar/\tau_e$, and 2) elastic reflection from the crystal potential in the final-state band gaps. The damping is described by complex k_{\perp}^f component of the final-state wavevector \mathbf{k}^f , with Imk_{\perp}^f connected to the photoelectron escape length λ as $2Imk_{\perp}^f = \lambda^{-1}$ (the factor of 2 comes from squaring the wavefunction amplitude for intensity).

The corresponding final-state dispersion $E^f(k_{\perp})$, shown in Fig.1 by black lines, is radically different from this one if the Bloch waves were undamped (propagating), as shown in gray: the dispersions as a function of Rek_{\perp}^f are smooth and *gapless*, passing continuously through the band gaps of the undamped $E(\mathbf{k})$ [3,5,9,10]. Such regions will in the following be somewhat loosely referred to as final-state band gaps. Note that due to surface-parallel invariance of the PE process the Bloch waves are undamped in the surface-parallel direction, retaining real \mathbf{k}_{\parallel} and gapped \mathbf{k}_{\parallel} -dispersions [5].

The final-state spectral function $A^f(E, \mathbf{k})$, due to the finite photoelectron lifetime, is in principle characterized by certain distribution in E . However, in the PE experiment this is reduced to the δ -function at the energy given by the PE analyser. Due to damping of the final-state wavefunction $A^f(E, \mathbf{k})$ is characterized, on the contrary, by Lorentzian distribution in real k_{\perp} , as shown in Fig.1, centered at $k_{\perp}^0 = Rek_{\perp}^f$ of the final-state Bloch wave and having the fullwidth $\delta k_{\perp} = 2Imk_{\perp}^f$ (in the angle-resolved PE experiment \mathbf{k}_{\parallel} is fixed and can be omitted). Therefore, $A^f(E, \mathbf{k})$ is given by

$$A^f(k_{\perp}) \propto \frac{\delta k_{\perp}}{(k_{\perp} - k_{\perp}^0)^2 + (\delta k_{\perp}/2)^2} \quad (1)$$

where the nominator stands for the normalization $\int_{-\infty}^{+\infty} A^f(k_{\perp}) dk_{\perp} = 1$. The final state of PE is thus characterized by *fixed E and broadening in k_{\perp}* whose width is determined by Imk_{\perp}^f of the damped final-state Bloch wave [1,2,8].

Nature of the PE initial state is different and complementary. The initial-state wavefunction is basically undamped: Removal of holes by the finite hole lifetime is compensated by their simultaneous generation by the electromagnetic field, which is almost homogeneous, extending into the crystal interior over a light absorption length of ~ 100 Å, very large compared to the final-state damping length. As sketched in Fig.1 (the lower panels represent the initial state), initial-state wavefunction is therefore described by an almost undamped Bloch wave, having well-defined real k_{\perp} .

The corresponding initial-state dispersion $E^i(k_{\perp})$ shows up sharp and *gapped* k_{\perp} -dispersions typical of the undamped states, radically different from the final-state.

The initial-state spectral function $A^i(E, \mathbf{k})$ is characterized, owing to well-defined k_{\perp} , by distribution in real k_{\perp} reduced to the δ -function. Due to finite hole lifetime τ_h it is characterized, on the contrary, by Lorentzian distribution in energy, as shown in Fig.1, centered at the band energy $E^i(k_{\perp})$ and having the fullwidth $\delta E = \hbar/\tau_h$. Therefore, $A^i(E, \mathbf{k})$ is given by

$$A^i(E) \propto \frac{\delta E}{(E - E^i(k_{\perp}))^2 + (\delta E/2)^2} \quad (2)$$

where the nominator ensures $\int_{-\infty}^{+\infty} A^i(E) dE = 1$. The initial state of PE is thus characterized, complementarily to the final state, by *fixed k_{\perp} and broadening in E* whose width is determined by the hole lifetime [1,2,8].

Note that some implementations of the one-step PE theory [7,11] describe the hole lifetime effects by damping of the initial states. However, such an approach is in clear contradiction with the PE experiment, which unambiguously finds in the valence band the gapped $E^i(k_{\perp})$ dispersions typical of undamped states. The same fundamental flaw is implied by an PE lineshape analysis (see, e.g., [12,13]) where the E -broadening of the initial state is replaced by an equivalent k_{\perp} -broadening $\sim \delta E \left(\frac{\partial E^i}{\partial k_{\perp}} \right)^{-1}$. Although such a replacement does not alter the lineshape while the k_{\perp} -dispersions remain linear, it leaves out some of the intrinsic effects discussed here.

Inverse photoemission (IPE) is commonly treated as the time-reversed PE process [14] in which the IPE final state in the conduction band is equivalent to the PE initial state in the valence band. However, the above arguments suggest a fundamental difference between the two:

as the IPE final state is excited by the damped LEED wavefunction, it is, in contrast to the PE initial state, also damped. Correspondingly, the conduction band $E(\mathbf{k})$ measured in the IPE experiment should be characterized by gapless k_{\perp} -dispersions similar to the PE final-state dispersions in Fig.1. Surprisingly, such a fundamental difference between the IPE and PE processes, tracing back to fundamental principles of quantum mechanics, has so far been addressed nor theoretically neither experimentally.

B. Development of the PE spectrum: Intrinsic k_{\perp} -resolution

We will now apply the above principles to analyze the PE response of 3D states. We will use a simple formalism based on interplay of the spectral functions [1,5,8], which is extremely simple and gives a clear physical insight. Its accuracy, despite principal limitations compared to the explicit one-step PE theory (see III E), is nevertheless sufficient for evaluation of the PE peak profiles [15].

As illustrated in Fig.2, the photoemission current $I(E^f, E^i)$ at the final-state energy E^f and initial-state energy $E^i = E^f - h\nu$ is formed by adding up the elementary photocurrents $dI(E^f, E^i)$ from all dk_{\perp} intervals, in which direct transitions take place, with k_{\perp} spanning the whole Brillouin zone (BZ). Each $dI(E^f, E^i)$ is weighted by the above spectral functions, $A^f(k_{\perp})$ to express closeness of k_{\perp} to k_{\perp}^0 of the final-state Bloch wave, and $A^i(E^i)$ to express closeness of E^i to the initial-state band energy $E^i(k_{\perp})$ at this k_{\perp} with δE varying along $E^i(k_{\perp})$. Moreover, each $dI(E^f, E^i)$ is multiplied by amplitude factors of the final-state surface transmission $|T^f|^2$ and photoexcitation matrix element $|M_{fi}|^2$. This yields $dI(E^f, E^i) = dk_{\perp} |T^f|^2 |M_{fi}(k_{\perp})|^2 A^f(k_{\perp}) A^i(E^i)$. To obtain the whole photocurrent, this expression should be integrated in k_{\perp} :

$$I(E^f, E^i) \propto \int_{-\infty}^{+\infty} dk_{\perp} |T^f|^2 |M_{fi}(k_{\perp})|^2 \frac{\delta k_{\perp}}{(k_{\perp} - k_{\perp}^0)^2 + (\delta k_{\perp}/2)^2} \frac{\delta E}{(E^i - E^i(k_{\perp}))^2 + (\delta E/2)^2}. \quad (3)$$

This integral can be evaluated at negligible computational cost (it can even be performed analytically using Taylor expansion of $E^i(k_{\perp})$ [5]).

Cuts of $I(E^f, E^i)$ along the $E^f = \text{const}$ line correspond to the constant-final-state (CFS) measurement mode, along the $h\nu = E^f - E^i = \text{const}$ line to the energy-distribution-curve (EDC) mode, and along $E^i = \text{const}$ to the constant-initial-state (CIS) mode. Fig.2 illustrates,

for simplicity, the PE spectrum taken using the CFS mode in which k_{\perp}^0 is constant throughout the spectrum.

The PE spectrum shows up, whichever the measurement mode, a peak centered roughly at the energy $E^i(k_{\perp}^0)$ dictated by the direct transition at k_{\perp}^0 between the final and initial bands. Broadening of the peak results from the final-state k_{\perp} -broadening combined with the initial-state E -broadening. In this context the k_{\perp} -broadening appears as an *intrinsic k_{\perp} -resolution* of the PE experiment (in the following we will use these terms interchangeably depending on the context). Note that this resolution, in contrast to the instrumentally limited resolution in \mathbf{k}_{\parallel} , is limited by intrinsic mechanisms involved in the PE process and can not be improved instrumentally.

C. Regimes of the PE experiment

If the k_{\perp} -resolution is at its best extreme $\delta k_{\perp} \rightarrow 0$, then $A^f(k_{\perp})$ becomes δ -function $\delta(k_{\perp} - k_{\perp}^f)$ and the integral (3) for $I(E^f, E^i)$ is reduced to $A^i(E)$ whose maximum points to the initial band energy $E^i(k_{\perp}^0)$ in the \mathbf{k} -point dictated by the direct transition. The PE peaks will then exactly follow the 3D quasiparticle dispersions in the valence band. In practice, such a situation is realized under the condition

$$\delta k_{\perp} \ll k_{\perp}^{BZ} \quad (4)$$

where k_{\perp}^{BZ} is the surface-perpendicular dimension of the BZ. This condition identifies the so-called *bandstructure regime* (BS-regime) of the PE experiment which ensures accurate 3D band mapping [2,6]. In the real space, it reads as $\lambda \gg c_{\perp}$, where c_{\perp} is the surface-perpendicular dimension of the unit cell.

If the PE final state comprise a few Bloch waves, the condition (4) should be generalized as $\delta k_{\perp} \ll \frac{k_{\perp}^{BZ}}{N}$, where N is the number of the corresponding final bands. Often in the literature (see, e.g., [6]) this number is confused with the number of *all* unoccupied bands available for given E^f and \mathbf{k}_{\parallel} ; as the latter becomes with energy progressively immense, an erroneous conjecture is made that at high energies any 3D band mapping is impossible. However, in the multitude of the available unoccupied bands only those are effective as the final bands, whose Bloch waves provide effective transport of the photoelectrons out of the solid by significant coupling to the outgoing plane wave [5,16]. Typically there are only a few ($N = 1 - 2$) final bands in this sense (see examples in III A).

If the k_{\perp} -resolution is at the opposite extreme $\delta k_{\perp} \rightarrow \infty$, any resolution in k_{\perp} is lost, $A^f(k_{\perp})$ becomes constant and the integral (3) yields, assuming that $|T^f|^2$ and $|M_{fi}|^2$ are independent of k_{\perp} and $E^i(k_{\perp})$ is linear, the 1-dimensional DOS (1DOS) $\frac{\partial k_{\perp}}{\partial E^i}$. The PE peaks will

then manifest the 1DOS maxima independently of k_{\perp}^0 . In practice, such a situation is achieved under the condition $\delta k_{\perp} \gtrsim k_{\perp}^{BZ}$, which identifies the so-called *1DOS-regime* [2,6].

Interpretation of the PE data between the bandstructure and 1DOS regimes is doubtful [6,17]: the PE peaks retain some $h\nu$ -dispersion, although damped by strong averaging in k_{\perp} , but they can be far from the true quasiparticle $E^i(k_{\perp})$.

Evolution of the regimes of the PE experiment with the k_{\perp} -resolution will now be illustrated by a PE simulation. The model employs the initial state whose parameters are chosen to resemble roughly the *sp*-band of Cu [5]: It is described by the free-electron dispersion $E^i(k_{\perp}) = \frac{\hbar^2}{2m}k_{\perp}^2 + V_{000}$ and the energy broadening δE varying linearly as a function of energy to match zero at the Fermi level E_F and an experimental value of 1.7 eV at the bottom of the band. The Fermi-Dirac cut is introduced as the ideal step function. The photocurrent $I(E^f, E^i)$ is evaluated by integration of the spectral functions in k_{\perp} (3), assuming constant amplitude factors $|T^f|^2$ and $|M_{fi}|^2$. The integration also extends above the Fermi vector k_{\perp}^F to include certain contribution from the tails of $A^i(E)$ in the unoccupied region of the valence band (see III B). For clarity, the PE spectra were evaluated for the CFS mode, in which k_{\perp}^0 is constant (deviations from the EDC mode are insignificant, because normally the final-state $\frac{\partial E^f}{\partial k_{\perp}}$ is large enough to ensure small variations of k_{\perp}^0 through the peak profile).

The simulation was performed for four δk_{\perp} values: zero for the ideal k_{\perp} -resolution, $0.2|\Gamma X|$ as a representative for the BS-regime in a real PE experiment, $0.6|\Gamma X|$ for degraded k_{\perp} -resolution, and $2|\Gamma X|$ for the 1DOS-regime. The results are shown in Fig.3 as series of the PE spectra with k_{\perp}^0 scanning along ΓX (upper panels, each series in different intensity scale) and positions of the spectral peaks mapped on top of the true valence band (lower panels).

In the ideal k_{\perp} -resolution limit the PE peak reflects the initial-state $A^i(E)$ and ideally follows the true $E^i(k_{\perp}^0)$. Interestingly, upon passing k_{\perp}^F there appears an extremely small peak just below E_F ; it replicates the low-energy tail of the spectral function $A^i(E)$ whose maximum is already above E_F (see III B).

In the BS-regime ($\delta k_{\perp} = 0.2|\Gamma X|$ in our simulation) the k_{\perp} -resolution remains sufficient for the PE peaks to closely follow $E^i(k_{\perp})$. This regime can be used for accurate 3D band mapping. Two peculiarities should be noted here: 1) Despite $A^i(E)$ becomes the δ -function upon approaching E_F , the PE peak does not sharpen up to singularity; 2) When k_{\perp}^0 passes k_{\perp}^F and enters into the unoccupied region, the peaks do not disappear but become 'ghost' peaks which are highly asymmetric and have their maximum stationary in energy just below E_F . Both peculiarities are appearances of the k_{\perp} -broadening

and will be analyzed in III B and III C.

As the k_{\perp} -resolution degrades ($\delta k_{\perp} = 0.6|\Gamma X|$), the concomitant averaging of $E^i(k_{\perp})$ causes asymmetry of the peaks and strong *intrinsic shifts* of their maxima from the true $E^i(k_{\perp})$. Although the PE peaks deceptively keep dispersion on k_{\perp}^0 , their use for 3D band mapping will return a distorted valence band dispersion. Note appearance of an additional shoulder-like structure, which originates from the large 1DOS in the bottom of the band and becomes notable as the main peak shifts upwards.

In the 1DOS-regime ($\delta k_{\perp} = 2|\Gamma X|$) the k_{\perp} -resolution is completely lost. The maxima of the PE peaks become stationary in energy reflecting the maximum of the valence band 1DOS (and a tiny replica of the $A^i(E)$ singularity at E_F , omitted from the plot). The k_{\perp}^0 changes show up only in the intensity modulation. Note however that the PE peaks are notably shifted from the true 1DOS maximum.

The regimes of the PE experiment in general follow the well-known "universal curve" $\lambda(E)$ [1,2,6] which gives the k_{\perp} -resolution as $\delta k_{\perp} = \lambda^{-1}$. The BS-regime holds while λ remains large, which takes place at low E^f below or not far above a plasmon excitation energy of 20-30 eV (see examples in III A). Upon further increase of energy λ reaches its minimum around 50-100 eV, and the PE experiment enters into the 1DOS-regime, although in practice the k_{\perp} -dispersion signatures are never completely suppressed. The BS-regime recovers in the high-energy region above ~ 300 eV where λ rises again (despite at these energies the unoccupied bands become immense in number, only one of them remains effective in the PE final state in the sense of effective coupling to the outgoing plane wave [16]).

The high-energy region is characterized by low PE intensity resulting from small valence band crossection and from the Debye-Waller factor, in which the increase of $h\nu$ reduces the PE intensity on equal footing with temperature. However, the advent of new high-brilliance synchrotron radiation sources and multidetection PE analysers has allowed for PE experiments in this region with reasonable count rates and resolution in E and \mathbf{k}_{\parallel} [18,19]. \mathbf{k} -resolved experiments were reported, for example, in [20] where the *sp*-band of Al was found to be mirrored in the $h\nu$ -dispersion of the PE signal up to 750 eV. Interestingly, this study has found an increase of the surface to bulk signal intensity ratio with $h\nu$, opposite to the tendency expected from the "universal curve", and attributed this surprising phenomenon to intrinsic phonon excitation effects involved in the PE process. These results call for further studies on the role of the phonon excitation in high-energy PE spectroscopy.

III. MECHANISMS LIMITING THE INTRINSIC ACCURACY

Degradation of the k_{\perp} -resolution, as we observed above, results in intrinsic shifts of PE peaks from the true valence band k_{\perp} -dispersions, limiting the *intrinsic accuracy* of 3D band mapping. These shifts can originate through various mechanisms, which will now be analyzed.

A. Non-linearity mechanism

Degradation of the k_{\perp} -resolution can crawl into the position of the PE peaks, firstly, by non-linearity of the valence band k_{\perp} -dispersion. As evident from Fig.2, in this case the integral number of the dk_{\perp} -intervals within the k_{\perp} -broadening will be different for the initial states whose E^i is above the direct-transition energy $E^i(k_{\perp}^0)$ and for the states whose E^i is below $E^i(k_{\perp}^0)$, being larger where the 1DOS is larger. Correspondingly, the PE peak becomes asymmetric. Its maximum somewhat shifts towards larger integral number of dk_{\perp} , deviating from the true $E^i(k_{\perp}^0)$. In the band interior the PE peaks shift towards the band edges, where the 1DOS is larger. Near the band edges the peaks, on the opposite, shift towards the band interior (so-called in-band shifting [4,5]) because beyond the band edge there are no states and the 1DOS is zero. We will refer to this mechanism to limit the intrinsic accuracy as the *non-linearity* mechanism. It was behind the intrinsic shifts observed in the PE simulation in Fig.3, where the PE peaks clearly followed the characteristic pattern of shifting towards larger 1DOS. Note that the intrinsic shifts due to the non-linearity mechanism depend, apart from δk_{\perp} and non-linearity of $E^i(k_{\perp})$, on the initial-state δE .

The non-linearity mechanism can be illustrated by experimental data for VSe₂ (for a detailed discussion see [4]). Information about the final-state dispersions and lifetimes, required for determination of δk_{\perp} , was achieved in this case by VLEED (see IV). The experimental energy dependence of V_i is shown in Fig. 4 (a). It is characterized by a sharp increases of V_i at the plasmon excitation energy $\hbar\omega_p$. The experimental $E^f(k_{\perp})$ is shown in Fig. 4 (b). Note that these final band can hardly be described by free-electron-like dispersions: there are *two* bands, and each can be free-electron fitted only locally with the inner potential strongly depending on E^f and \mathbf{k}_{\parallel} (such a complicated structure of the final states is in fact typical of many materials with large unit cell, containing more than one atom, due to backfolding of many free-electron bands into the first BZ and their mutual hybridization). An estimate of δk_{\perp} was obtained, neglecting some increase in the final-state band gaps, as $2V_i \left(\frac{\partial E^f}{\partial k_{\perp}} \right)^{-1}$ (see IV). The obtained δk_{\perp} values are shown in Fig. 4 (b) superimposed on the final bands.

Following the increase of V_i , the k_{\perp} -resolution degrades above $\hbar\omega_p$. The results of PE band mapping, the binding energy of the PE peaks as a function of k_{\perp}^0 , are shown in Fig. 4 (c) with distinction for the final states below and above $\hbar\omega_p$. Near the band edges of the 3D bands the experimental points above $\hbar\omega_p$ are systematically shifted towards the band interior compared to those below $\hbar\omega_p$. It should be stressed that here we have an explicit example how *the same* initial states yield *different* energies of the PE peaks depending on the k_{\perp} -resolution. The observed shifts demonstrate the intrinsic effect of in-band shifting, occurring mainly by the non-linearity mechanism. Interestingly, increase of E^f towards 50 eV results in further increase of δk_{\perp} and suppression of any dispersion of the PE peaks [21].

Our analysis demonstrates that for VSe₂ the energy region of accurate 3D band mapping is exhausted by low E^f below or not far above $\hbar\omega_p$. Such a situation is in fact fairly general, because a pronounced plasmon threshold is typical of many materials with some exceptions such as Cu and Ni. The intrinsic accuracy effects similar to VSe₂ were also observed for TiS₂ [4], WSe₂ [22], Ge [17], etc.

In the final-state band gaps the Bloch waves experience additional damping due to elastic scattering from the crystal potential [5,23]. Although this is normally much weaker than the damping due to V_i , as in the above example, for materials with exceptionally large final-state band gaps the additional damping can cause notable degradation of the k_{\perp} -resolution. Graphite is a typical example of this (for a detailed discussion see [24,25]). Its final bands were simulated using the empirical pseudopotential method based on the VLEED data for their energies in the Γ -point (the simulation is therefore less accurate in the BZ interior) and V_i . The resulting $E^f(k_{\perp})$ is shown in Fig.5 (a) and (b) as a function of Imk_{\perp}^f and Rek_{\perp}^f , respectively, using the double-BZ representation to reflect the dipole selection rules in graphite. The final states are characterized by a strong increase of $\delta k_{\perp} = 2Imk_{\perp}^f$ in the two band gaps in the Γ -point. Based on these data, we simulated the PE response of the valence π -band, having the 3D character, using the same formalism (3). The results are shown in Fig.5 (b). When the final-state k_{\perp}^0 moves towards the Γ -point and enters the band gaps, progressive degradation of the k_{\perp} -resolution results, by the non-linearity mechanism, in increasing of the in-band shifts. In the lower band gap, which has the maximal width, the increase of δk_{\perp} is particularly strong; the concomitant in-band shifting is so dramatic that it overcomes the trend dictated by the band dispersions themselves and *reverses* the dispersion of the PE peaks compared to the true π -band. Such an unusual reversed dispersion has indeed been found in the PE experiment [25].

Typically, intrinsic shifts near the band extrema due

to the non-linearity mechanism are of the order of a few tenths of eV. The experiment often suggests however larger shifts [4,21,22]. As degradation of the k_{\perp} -resolution goes along with reduction of the escape length λ , this reveals certain contribution of surface effects such as suppression of the 1DOS in the band extrema (see IIID). It should be noted that the condition (4) identifying the BS-regime is particularly restrictive for layered materials owing to their small k_{\perp}^{BZ} (see [26] for a specialized survey).

B. 'Ghost' peaks at E_F

An interesting phenomenon occurs when a 3D band crosses the Fermi surface. This situation is described by the PE simulation in Fig.3: When the direct-transition k_{\perp}^0 moves outside the Fermi surface and starts sampling the unoccupied part of the valence band, the PE peaks, mysteriously, do not disappear. Instead, they become asymmetric and stationary in energy just below the Fermi level E_F , and only gradually reduce in amplitude. Experimentally, such a phenomenon has been observed, for example, in a famous PE study on Na, where the *sp*-band crosses E_F [27,28]. We will refer to this phenomenon as '*ghost*' peaks. It has in fact two contributions due to different mechanisms.

The first contribution is due to a general mechanism taking place for 3D as well as 2D bands. It comes from the *unoccupied* states next to E_F : The spectral function $A^i(E)$, centered at the band energy above E_F , protrudes its low-energy tail, however small the remaining amplitude, below E_F and gives therefore some PE intensity (such an effect for 2D bands is discussed, for example, in [29,30]). Such a contribution can be isolated in our PE simulation by restricting the integration (3) to $k_{\perp} > k_{\perp}^F$. It survives even in the limit of the ideal k_{\perp} -resolution, see Fig.3. In any case, the '*ghost*' peak intensity due this mechanism is very small.

The second contribution, much predominating for the 3D bands, comes from the occupied states: As illustrated in Fig.6, even if k_{\perp}^0 moves outside the Fermi surface, the dk_{\perp} -states at the initial-state E^i below E_F give certain '*ghost*' intensity by virtue of being accessible via the k_{\perp} -broadening. Upon moving k_{\perp}^0 further from k_{\perp}^F the $A^f(k_{\perp})$ profile shifts, reducing its amplitude at the initial band and, concomitantly, the '*ghost*' peak amplitude. Note that this mechanism gives a significant '*ghost*' peak intensity even if the initial-state E -broadening is vanishing which takes place upon approaching E_F .

The '*ghost*' peak phenomenon complicates identification of the E_F crossings in mapping of the Fermi surface formed by 3D bands. A well-known example is NbSe₂, whose $4p_z$ band forms a 3D pocket of the Fermi surface with extension in k_{\perp} small compared to the k_{\perp} -broadening; direct mapping of this pocket is precluded

by non-dispersive '*ghost*' intensity [31,32]. Even if the mapping is performed as a function of \mathbf{k}_{\parallel} , the '*ghost*' peaks stay at E_F through the entire interval of \mathbf{k}_{\parallel} where at least some part of the 3D band remains occupied. It should be noted that often the PE data, especially for quasi-2D materials, is interpreted neglecting the 3D effects; in this case such '*ghost*' peaks in the \mathbf{k}_{\parallel} -dispersion are misinterpreted as a sign of unusual self-energy effects. A way to circumvent the '*ghost*' peak problem in the Fermi surface mapping was suggested in [5]: one varies \mathbf{k}_{\parallel} , simultaneously changing E^f to remain in the $E^i(k_{\perp})$ minimum.

C. Linewidths near E_F

Similar in origin to the '*ghost*' peaks is an interesting PE linewidth behavior upon approaching E_F : As seen in our simulations in Fig.3 for the BS-regime, the PE peak from the 3D band, mysteriously, retains a finite linewidth up to E_F without sharpening up as might be expected from the behavior of the initial-state $A^i(E)$, which becomes singular at E_F because of the vanishing E -broadening. The origin of such a counter-intuitive linewidth behavior is again due to the 3D character of the band and the k_{\perp} -broadening [13,33]: As one can conjecture from Fig.6, even if the E -broadening is zero, the initial states around the direct-transition energy $E^i(k_{\perp}^0)$ are accessible via the k_{\perp} -broadening and contribute to the PE peak width. In the ideal k_{\perp} -resolution limit, as demonstrates our simulation in Fig.3, the PE peak well becomes singular towards E_F .

An experimental example of such an effect of the k_{\perp} -broadening on the linewidths can be seen, for example, in the PE peak from the *sp*-band of Cu whose linewidth increases upon approaching E_F [15]. In [13,33] it was shown that the same effect can explain an unusual linewidth energy dependence near E_F observed in Bi₂Sr₂CaCu₂O₈, which otherwise would indicate deviations from the Fermi liquid picture.

Significant PE intensity next to E_F , seen in all regimes of the simulation in Fig.3, also originates from existence of a 3D band crossing E_F and the k_{\perp} -broadening. Such a peculiarity is typical of the PE experiments on 3D materials such as Cu.

D. Other mechanisms

Intrinsic shifts in the 3D bands can also appear due to a *matrix element* mechanism: If M_{fi} as a function of energy and k_{\perp} undergoes sharp variations within the k_{\perp} -broadening, a contribution of the states above and below $E^i(k_{\perp}^0)$ is different (see Fig.2). The peak becomes asymmetric and it maximum experiences an intrinsic shift from the true band energy. Such a mechanism has been

identified, for example, in TiS_2 [4]. Similar effects due to T^f should be less pronounced, because the energy variations of T^f are normally smooth and become sharper only at extremely low E^f , as can be seen in VLEED data (see, e.g., [4,24,34]).

The above mechanisms were all based on the bulk bandstructure picture, in which the bandstructure near the surface is considered identical to the bulk one. This implies that the crystal potential, and thus the wavefunctions, ideally repeat the bulk ones up to the surface. In fact, within a few atomic layers of the PE escape depth they can experience notable modification. Such *surface effects* also give rise to intrinsic shifts. For example, the 1DOS singularities in the band extrema, characteristic of the bulk $E(\mathbf{k})$, are smeared in the local DOS near the surface (see, e.g., [35–37]), which results in an increase of the in-band shifting. The surface effects are harder to control compared to the k_\perp -resolution effects. Qualitatively, their contribution reduces with increase of λ simultaneously with reduction of the intrinsic shifts of the bulk origin due to the concomitant improvement of the k_\perp -resolution.

Surface photoelectric effect, generated by abrupt change in the dielectric response at the surface barrier and described by the $\nabla \cdot \mathbf{A}$ part of M_{fi} , can influence the PE signal from the 3D bands through interference of the surface and bulk PE components (see, e.g., [38–40]). Normally this effect only causes some asymmetry of the PE peaks. However, near the surface and bulk plasmon excitation energies, especially for free-electron metals such as Na, the lineshape changes can be drastic and return large intrinsic shifts [28,41]. In [40] it was demonstrated that the surface and bulk components can be experimentally separated by changing the light incidence angle.

E. Intrinsic accuracy within the one-step PE theory

The intrinsic effects are naturally embodied in the one-step PE theory (see, e.g., [6,7]) which finds the PE intensity as a matrix element $|\langle \Phi^f | \hat{\mathbf{A}} \cdot \hat{\mathbf{p}} | \Phi^i \rangle|$ between the final- and initial-state wavefunctions Φ^f and Φ^i . Interference between different Bloch wave constituents in the final and initial states, matrix element effects and surface effects, all ignored in the simplified formalism (3) used above, are naturally included here. However, a heavy computational machinery often obscures the physical mechanisms.

An example of the intrinsic accuracy analysis using the one-step PE theory can be found in [42] in application to TiSe_2 . Similarly to the above results for VSe_2 , for the final states above $\hbar\omega_p$ the k_\perp -resolution was found to degrade, causing strong broadening and intrinsic shifts of the PE peaks. Surface effects due to smearing of the bulk 1DOS singularities have also been identified. Another

example is a calculation on Na [28], which described the 'ghost' peaks at E_F and in-band shifting in the bottom of the valence band.

IV. OPTIMIZATION OF THE PE EXPERIMENT USING VLEED

3D band mapping remains relevant if the intrinsic shifts are small. Of the factors affecting these shifts, the non-linearity of the k_\perp -dispersion, initial-state E -broadening and, partly, variations of M_{fi} are all due to inherent properties of the valence bands under study and remain beyond control by the experimentator. The k_\perp -resolution, on the contrary, is an exclusively final-state property, and by tuning E^f can be taken to values which ensure negligible intrinsic shifts. This is achieved in the BS-regime $\delta k_\perp \ll k_\perp^{BZ}$ (see II C). The exact energy ranges of this regime are however much material dependent. Knowledge of the k_\perp -resolution energy dependence is therefore required.

VLEED, covering the energy range below ~ 40 eV, has recently been established as the experimental method giving the most direct access to the PE final states with resolution in the 3D wavevector (see [3–5] and references therein). In the VLEED spectra of elastic electron reflection, the energies of the spectral structures give the critical points in the final bands. $E^f(k_\perp)$, obtained from this experimental data, can further be used to control k_\perp in the PE experiment. Broadening of the VLEED structures, moreover, gives an estimate of the corresponding V_i values [4,34,43]. By performing calculations of the complex bandstructure with the experimental V_i [3,5,34], one obtains the k_\perp -resolution as $\delta k_\perp = 2Imk_\perp^f$ of the generated Bloch waves (and simultaneously the energy dependence of λ , as it was recently demonstrated for graphite in comparison with determination of λ by the conventional overlayer method [43]). As such calculations can however be time-consuming, δk_\perp can be estimated in a simplified manner directly from the V_i values and the final-state group velocity $\frac{\partial E^f}{\partial k_\perp}$ as [9,12,13]

$$\delta k_\perp \sim 2V_i \left(\frac{\partial E^f}{\partial k_\perp} \right)^{-1} \quad (5)$$

This estimate is accurate however only outside the final-state band gaps. Nevertheless, increase of δk_\perp associated with additional damping in the gaps (see Fig.5) is normally less significant, except for a few materials with exceptionally wide band gaps such as graphite.

Use of the VLEED predictions on the k_\perp -resolution allows the experimentator to *optimize* the PE experiment on the intrinsic accuracy by selecting the E^f intervals which ensure the BS-regime (see the examples in III A).

As a concluding remark, it should be noted that one can significantly improve accuracy of 3D band mapping

by computational modelling of the intrinsic accuracy effects, as described above, and correcting the experimental data correspondingly. This is often critical for proper evaluation of the true excited-state self-energy effects, for example in graphite [25] and Na [28].

V. CONCLUSION

Fundamental principles of PE have been analysed, focussing on emission from 3D states in the valence band. Damping of the final state due to inelastic and elastic scattering in the crystal results in equivalent broadening in k_{\perp} , which acts as the intrinsic k_{\perp} -resolution of the PE experiment. The PE peak is then formed as a matrix-element weighted average of the quasiparticle k_{\perp} -dispersion in valence band, which can be shifted from the dispersion itself. Such shifts intrinsically limit the accuracy of 3D band mapping, which remains accurate only in the bandstructure regime, characterized by the intrinsic k_{\perp} -broadening small compared to the BZ extension in k_{\perp} . Upon degradation of the k_{\perp} -resolution the PE experiment yields increasing intrinsic shifts and, finally, enters into the 1DOS regime. The intrinsic k_{\perp} -resolution can be controlled using VLEED, which gives the final-state dispersions and lifetimes. The mechanisms forming the intrinsic shifts have been exposed, including non-linearity of the k_{\perp} -dispersion, variations of the matrix element and surface effects. Appearance of the intrinsic shifts and transformation of the regimes of the PE experiment has been analysed using a physically transparent picture of interplay of the final- and initial-state spectral functions, and illustrated by PE simulations and experimental examples. The k_{\perp} -broadening gives rise to other surprising effects typical of 3D valence states such as 'ghost' peaks whose direct-transition k_{\perp} falls outside the Fermi surface, and finite width of the PE peaks at the Fermi level.

I thank R. Claessen, P.O. Nilsson and R. Feder for promoting discussions. Financial support by the Deutsche Forschungsgemeinschaft (CL124/5-1) is gratefully acknowledged.

- [3] V.N. Strocov, H. Starnberg and P. O. Nilsson, *J. Phys.: Cond. Matter* **8**, 7539 (1996); *Phys. Rev. B* **56**, 1717 (1997)
- [4] V.N. Strocov, H.I. Starnberg, P.O. Nilsson, H.E. Brauer and L.J. Holleboom, *Phys. Rev. Lett.* **79** (1997) 467; *J. Phys. Condens. Matter* **10** (1998) 5749
- [5] V.N. Strocov, R. Claessen, G. Nicolay, S. Hüfner, A. Kimura, A. Harasawa, S. Shin, A. Kakizaki, H.I. Starnberg, P.O. Nilsson and P. Blaha, *Phys. Rev. Lett.* **81** (1998) 4943; *Phys. Rev. B* **63** (2001) 205108
- [6] P.J. Feibelman and D.E. Eastman, *Phys. Rev. B* **10** (1974) 4932
- [7] J.B. Pendry, *Surf. Sci.* **57** (1976) 679
- [8] R. Matzdorf, *Appl. Phys. A* **63** (1996) 549; *Surf. Sci. Rep.* **30** (1998) 153
- [9] J.B. Pendry, *J. Phys. C: Solid State Phys.* **2** (1969) 2283
- [10] J.B. Pendry, *Low Energy Electron Diffraction* (Academic Press, London, 1974)
- [11] P.O. Nilsson, J. Kanski and C.G. Larsson, *Solid State Commun.* **36** (1980) 111
- [12] J.A. Knapp, F.J. Himpsel and D. E. Eastman, *Phys. Rev. B* **19** (1979) 4952
- [13] N.V. Smith, P. Thiry and Y. Petroff, *Phys. Rev. B* **47** (1993) 15 476
- [14] J.B. Pendry, *Phys. Rev. Lett.* **45** (1980) 1356
- [15] K. Berge, A. Gerlach, G. Meister, A. Goldmann and J. Braun, *Surf. Sci.* **498** (2002) 1
- [16] V.N. Strocov, *Solid State Commun.* **106**, 101 (1997)
- [17] W.D. Grobman, D.E. Eastman, J.L. Freeouf, *Phys. Rev. B* **12** (1975) 4405
- [18] Y. Saitoh, H. Kimura, Y. Suzuki, T. Nakatani, T. Matsushita, T. Muro, T. Miyahara, M. Fujisawa, K. Soda, S. Ueda, H. Harada, M. Kotsugi, A. Sekiyama and S. Suga, *Rev. Sci. Instr.* **71** (2000) 3254
- [19] T. Matsushita, T. Muro, Y. Saitoh, T. Nakatani, A. Sekiyama and S. Suga, *Surf. Rev. and Lett.* **9** (2002) 1321
- [20] P. Hofmann, C. Søndergaard, S. Agergaard, S.V. Hoffmann, J.E. Gayone, G. Zampieri, S. Lizzit and A. Baraldi, *Phys. Rev. B* **66** (2002) 245422
- [21] H.I. Starnberg, H.E. Brauer, P.O. Nilsson, L.J. Holleboom and H.P. Hughes, *Mod. Phys. Lett.* **8** (1994) 1261
- [22] Th. Finteis, M. Hengsberger, Th. Straub, K. Fauth, R. Claessen, P. Auer, P. Steiner, S. Hüfner, P. Blaha, M. Vögt, M. Lux-Steiner and E. Bucher, *Phys. Rev. B* **55** (1997) 10 400; *ibid.* **59** (1999) 2461
- [23] R. Courths, H. Wern, G. Leschik and S. Hüfner, *Z. Phys. B* **74**, 233 (1989)
- [24] V.N. Strocov, P. Blaha, H.I. Starnberg, M. Rohlfing, R. Claessen, J.-M. Debever and J.-M. Themlin, *Phys. Rev. B* **61** (2000) 4994
- [25] V.N. Strocov, A. Charrier, J.-M. Themlin, M. Rohlfing, R. Claessen, N. Barrett, J. Avila, J. Sanchez and M.-C. Asensio, *Phys. Rev. B* **64** (2001) 075105
- [26] V.N. Strocov, in *Electron spectroscopies applied to low-dimensional materials* (Kluwer, Netherlands, 2000)
- [27] E. Jensen and E.W. Plummer, *Phys. Rev. Lett.* **55** (1985) 1912
- [28] K.W.-K. Shung and G.D. Mahan, *Phys. Rev. Lett.* **57**, 1076 (1986)
- [29] R. Claessen, R.O. Anderson, J.W. Allen, C.G. Olson, C.

* Email F1XVS@fy.chalmers.se. Also with the Institute for High-Performance Computations and Data Bases, St.Petersburg

- [1] *Angle-Resolved Photoemission*, edited by S.D. Kevan (Elsevier, Amsterdam, 1992)
- [2] S. Hüfner, *Photoelectron Spectroscopy* (Springer, Berlin, 1995)

Janowitz, W.P. Ellis, S. Harm, M. Kalning, R. Manzke and M. Skibowski, Phys. Rev. Lett. **69** (1992) 808

[30] R. Claessen, R.O. Anderson, G.-H. Gweon, J.W. Allen, W.P. Ellis, C. Janowitz, C.G. Olson, Z.X. Shen, V. Eyert, M. Skibowski, K. Friemelt, E. Bucher, S. Hüfner, Phys. Rev. B **54** (1996) 2453

[31] V.N. Strocov, Th. Fintais, R. Claessen, G. Nicolay, D. Ehm, V. Colbus, S. Hüfner, H. Starnberg and V. Eyert, *BESSY Annual Rep.* (1997) 219

[32] K. Rossnagel, O. Seifarth, L. Kipp, M. Skibowski, D. Voss, P. Krüger, A. Mazur and J. Pollmann, Phys. Rev. B **64** (2001) 235119

[33] N.V. Smith, *Comments Cond. Mat. Phys.* **15** (1992) 263

[34] E.E. Krasovskii, W. Schattke, V.N. Strocov and R. Claessen, Phys. Rev. B **66** (2002) 235403

[35] E. Pehlke and W. Schattke, J. Phys. C: Solid State Phys. **20** (1987) 4437

[36] C.M. Fang, R.A. de Groot and C. Haas, Phys. Rev. B **56**, 4455 (1997)

[37] R. Courths, M. Lau, T. Scheunemann, H. Gollisch and R. Feder, Phys. Rev. B **63** (2001) 195110

[38] H.J. Levinson, E.W. Plummer and P.J. Feibelman, Phys. Rev. Lett. **43** (1979) 952

[39] E.D. Hansen, T. Miller and T.-C. Chiang, Phys. Rev. Lett. **78** (1997) 2807

[40] T. Michalke, A. Gerlach, K. Berge, R. Matzdorf and A. Goldmann, Phys. Rev. B **62** (2000) 10544

[41] D. Claesson, S.-Å. Lindgren, L. Walldén and T.-C. Chiang, Phys. Rev. Lett. **82** (1999) 1740

[42] E. Pehlke and W. Schattke, Solid State Commun. **69** (1989) 419

[43] N. Barrett, E.E. Krasovskii, J.-M. Themlin and V.N. Strocov, Phys. Rev. B (in press)

FIG. 1. Characteristic behavior of wavefunctions, k_{\perp} -dispersions and spectral functions of the final and initial states of PE, shown, respectively, on the upper and lower panels. The final states are characterized by fixed E and broadening in k_{\perp} , while the initial state, complementarily, by fixed k_{\perp} and broadening in E .

FIG. 2. Development of the PE peak. Its broadening results from the final-state k_{\perp} -broadening, defining the intrinsic k_{\perp} -resolution δk_{\perp} , combined with the initial-state E -broadening δE . The maximum of the peak shows an intrinsic shift towards the larger average 1DOS from the position $E^i(k_{\perp}^0)$ dictated by the direct transition at k_{\perp}^0 .

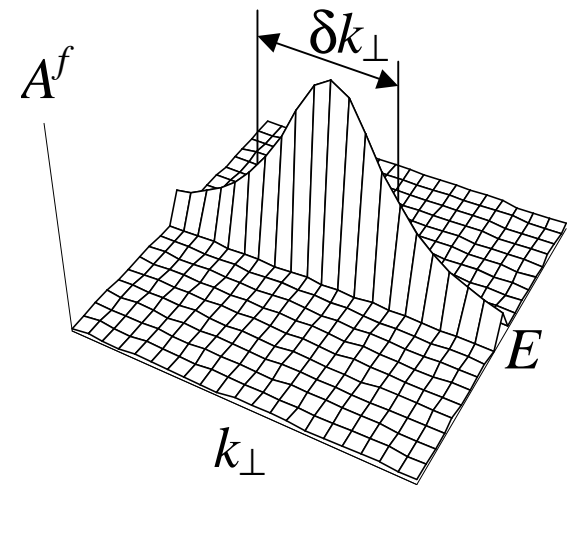
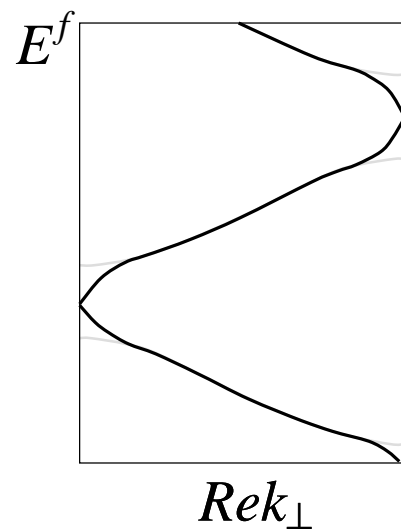
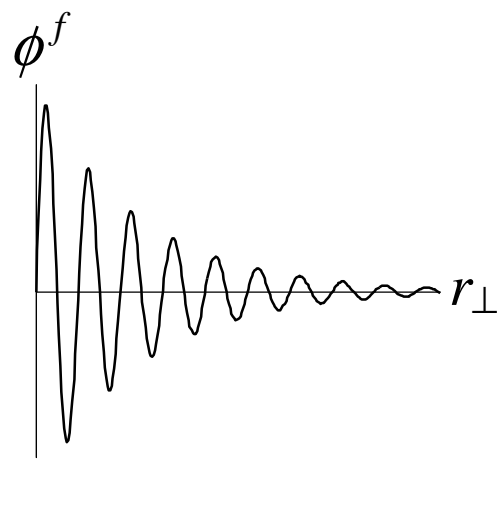
FIG. 3. Simulated PE experiments on a model 3D band, resembling the sp -band of Cu, performed with different strength of damping in the final state. The corresponding δk_{\perp} values of the intrinsic the k_{\perp} -resolution (indicated on top) are characteristic of the BS-regime (left), degraded k_{\perp} -resolution (center), and 1DOS-regime (right). The results are shown as series of a few PE spectra (upper panels) whose offsets reflect scanning of the direct-transition k_{\perp}^0 along ΓX , and the position of the spectral peak maxima on top of the true valence band $E^i(k_{\perp})$ (lower panels). Finite width of the PE peak upon approaching E_F and 'ghost' peaks remaining after the E_F crossing as both effects of the k_{\perp} -broadening. Degradation of the k_{\perp} -resolution results in intrinsic shifts of the PE peaks, in this case is due to the non-linearity mechanism, from the true valence band.

FIG. 4. Intrinsic accuracy for VSe₂: (a) Energy dependence of the final-state V_i with a characteristic increase due to the plasmon excitation at $\hbar\omega_p$; (b) Final-state bands (including, of all unoccupied bands, only those whose Bloch wave effectively couples to the outgoing photoelectron plane wave). The k_{\perp} -resolution is shown by shading; (c) Position of the PE peaks superimposed on DFT-LAPW calculations. The points obtained with E^f below $\hbar\omega_p$ are shown as solid dots, and above as open dots. A systematic in-band shifting in the 3D bands, following degradation of the k_{\perp} -resolution above $\hbar\omega_p$, is mainly due to the non-linearity mechanism.

FIG. 5. Intrinsic accuracy for graphite: (a,b) Empirical pseudopotential simulation of the final bands based on VLEED data (black lines); the band gaps are emphasized by setting V_i to zero (gray); (c) Simulated position of the PE peaks (dense dots) from the valence π -band on top of its true dispersion. Severe degradation of the k_{\perp} -resolution $\delta k_{\perp} = Imk_{\perp}^f$ in the final-state band gaps causes large in-band shifts due to the non-linearity mechanism, and even reverses the dispersion of the PE peaks in the lower gap.

FIG. 6. Mechanism of the 'ghost' peaks from 3D bands crossing the Fermi surface. Even if the direct-transition k_{\perp}^0 is in the unoccupied region, the PE signal comes from the occupied part of the valence band accessible via the final-state k_{\perp} -broadening.

final state



initial state

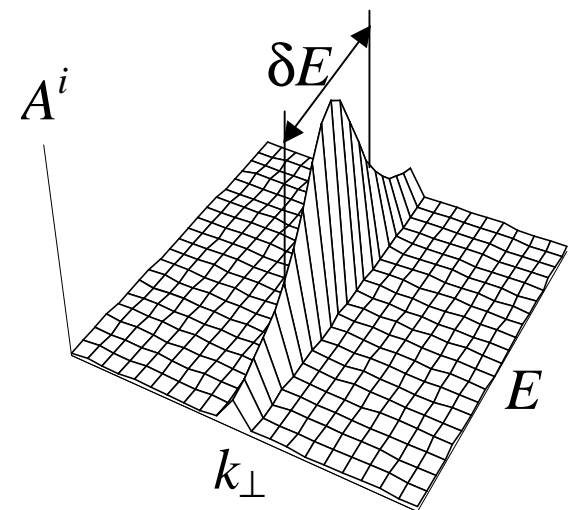
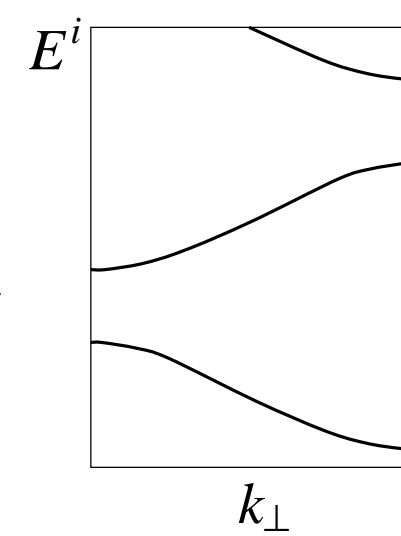
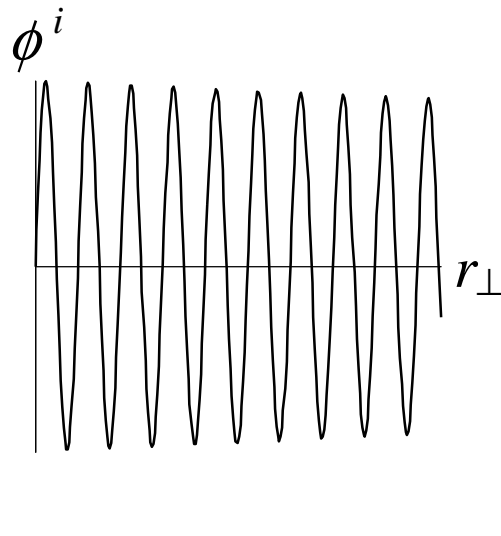


Fig.1byV.N.Strocov

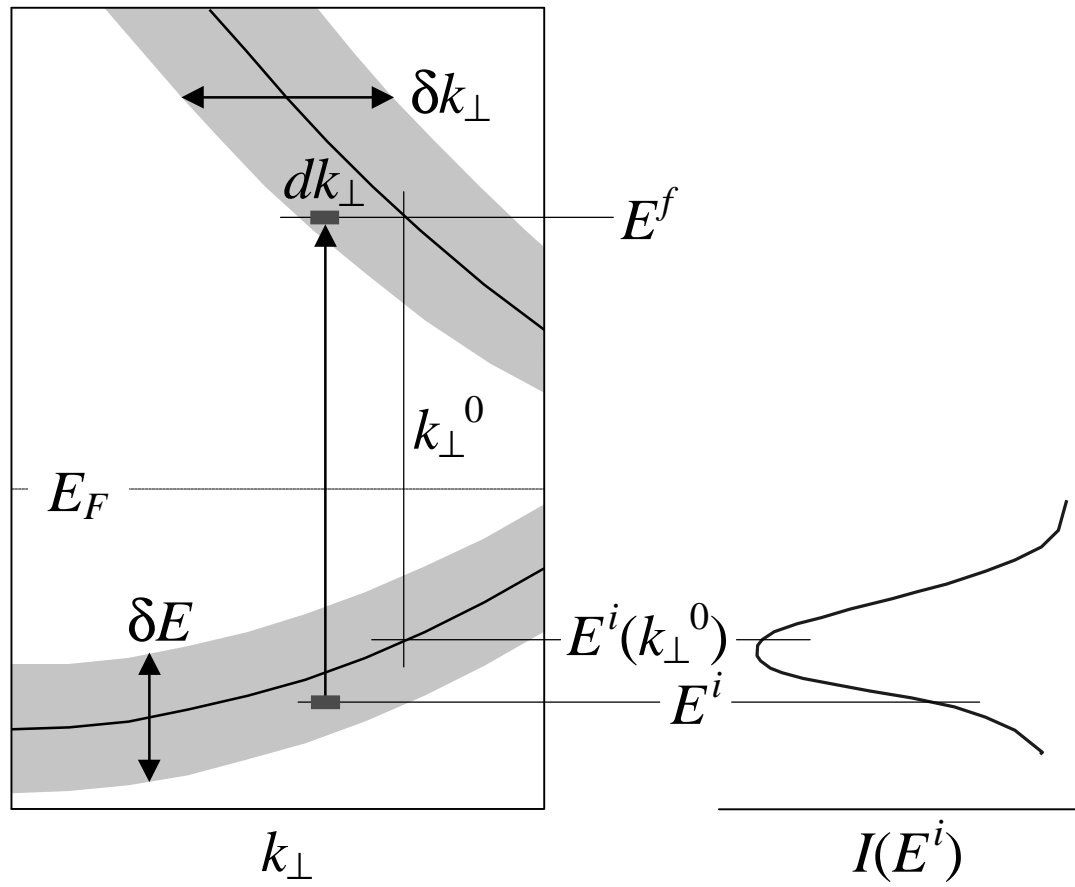


Fig.2 by V.N.Strocov

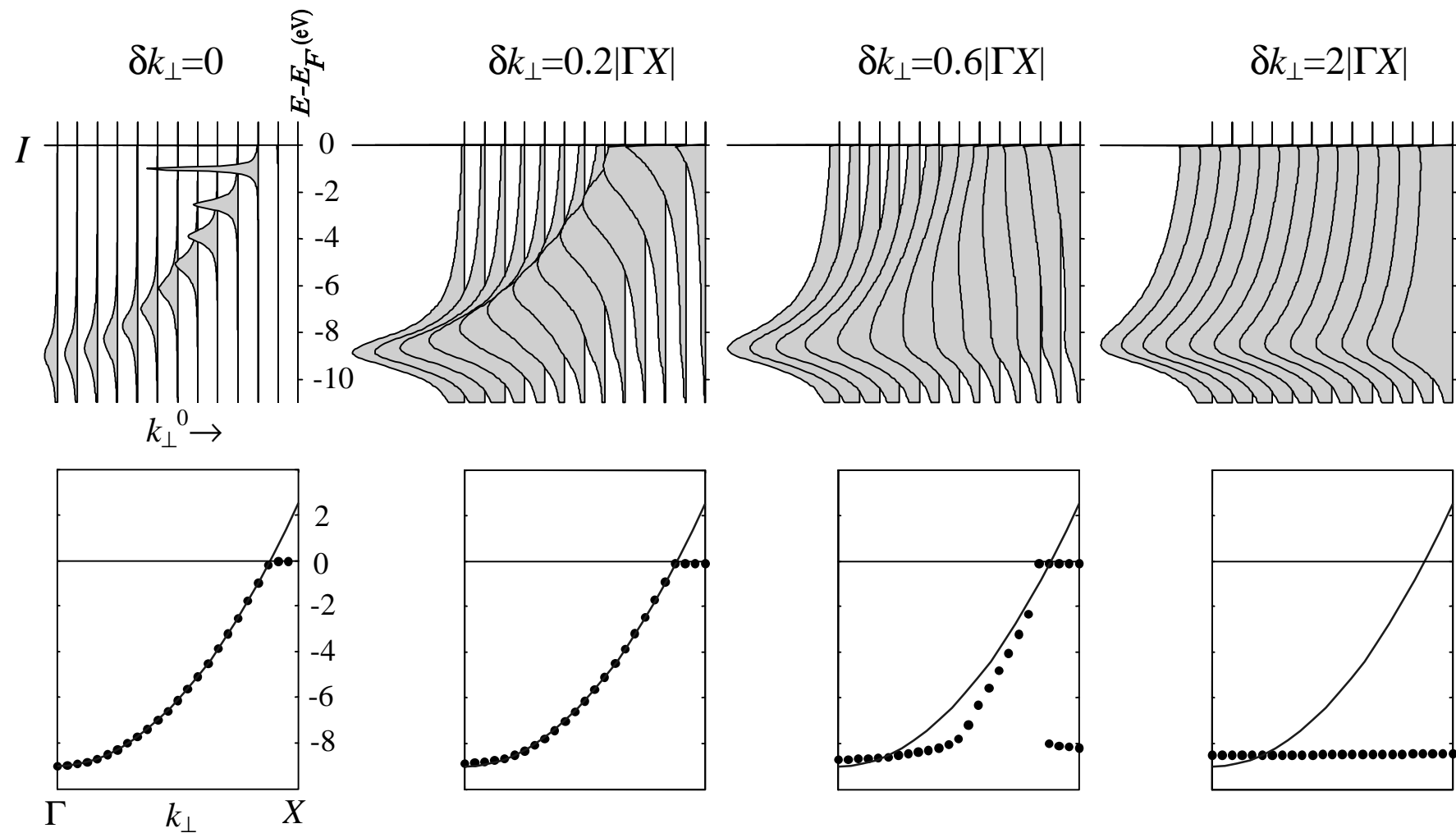


Fig.3byV.N.Strocov

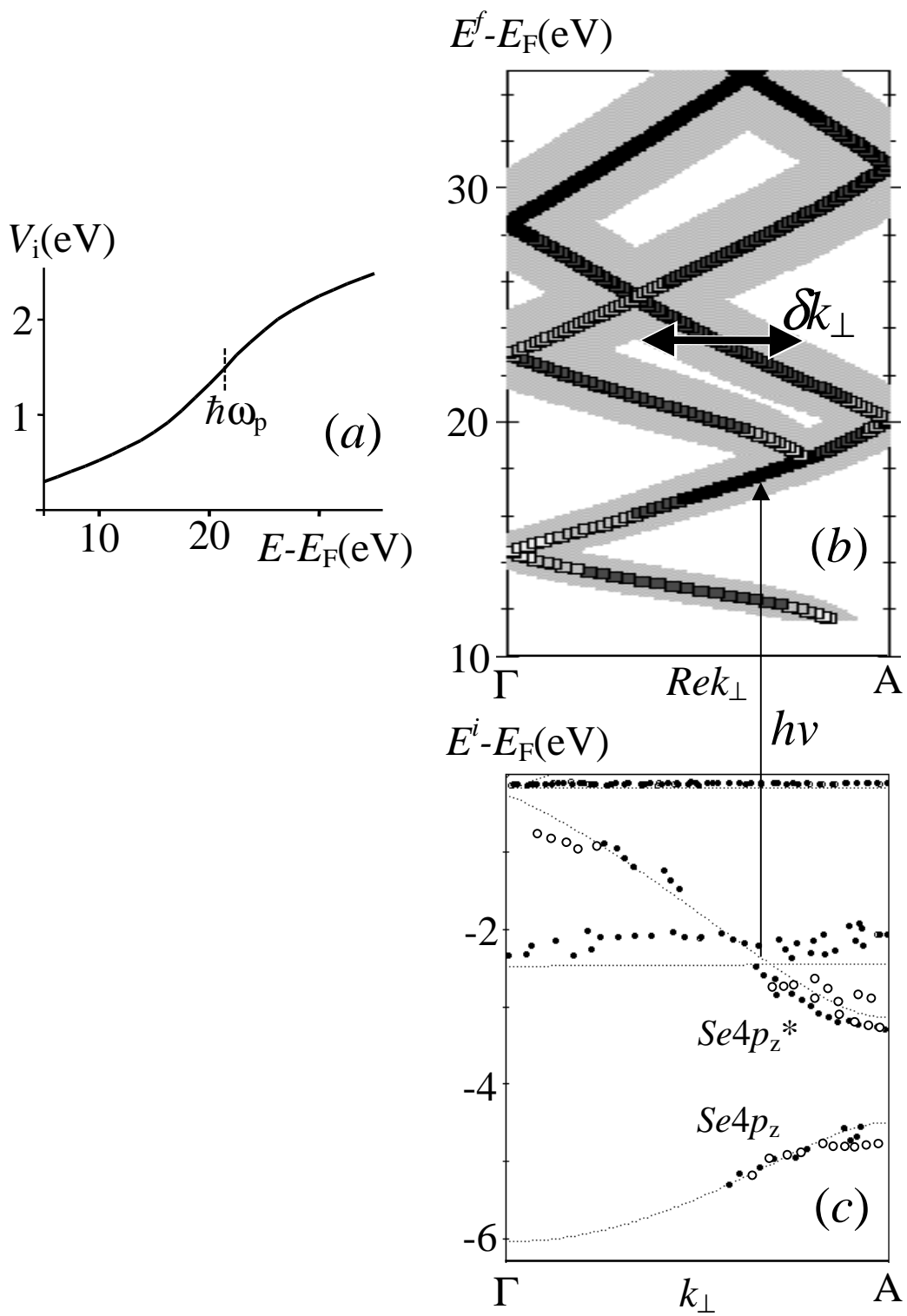


Fig.4 by V.N.Strocov

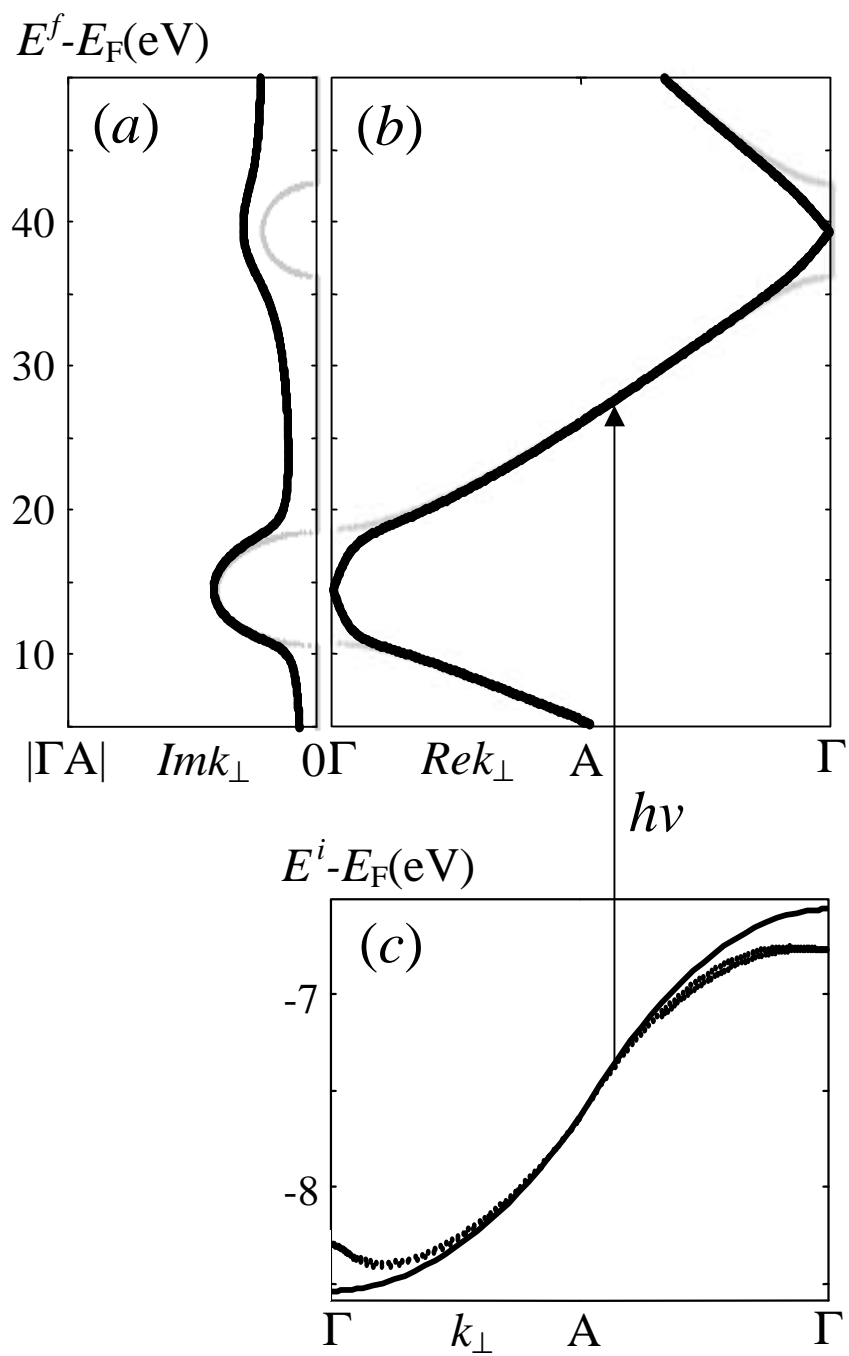


Fig.5 by V.N.Strocov

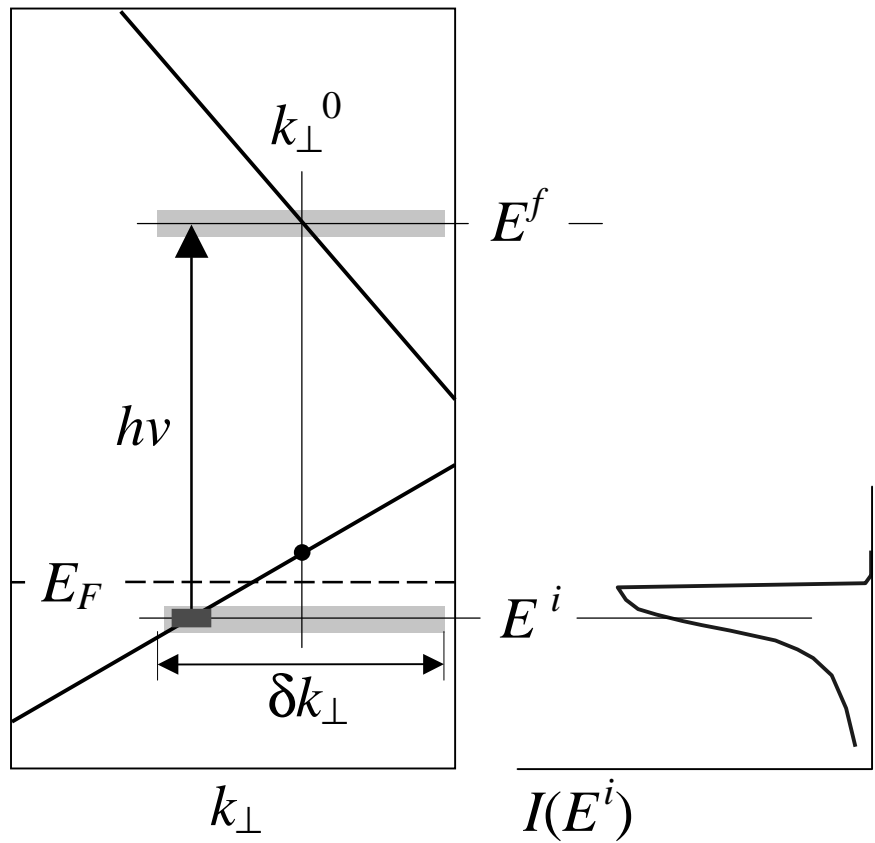


Fig.6 by V.N.Strocov